

Accurate and Efficient Computation of the Inductance Matrix of Transformer Windings for the Simulation of Very Fast Transients

Pablo Gómez, *Member, IEEE*, and Francisco de León, *Senior Member, IEEE*

Abstract—When a transformer is subjected to very fast front transients, the penetration of the magnetic flux into the core becomes, in general, negligible. To represent this phenomenon, it is common practice to compute the winding inductance matrix (turn-to-turn) at very high frequencies using the expressions for air-core inductors. However, since the core becomes a magnetic insulating wall at very high frequencies (MHz), the distribution of the magnetic field is altered because the field cannot enter the region occupied by the core. Therefore, the air-core approximation formulae overestimate the inductance at high frequencies. This is especially true in the region inside the core window. Large errors are found when the inductances are computed with the air-core approximation. This paper presents a technique, based on the application of a multilayer method of images, to take the presence of the core into consideration. The final expressions are very simple, yet they give remarkably accurate results. Comparisons with finite-element analyses prove the excellent accuracy of the technique.

Index Terms—Inductance matrix, magnetic fields, method of images, transformer windings, very fast transients.

I. INTRODUCTION

FAST and very fast front transients in transformers are commonly studied using internal models. These models consider the propagation and distribution of the incident surge along the transformer windings [1]–[11]. Inductive, capacitive, and loss components are needed to accurately describe the behavior of windings at high frequencies.

The required detail of winding models for the analysis of fast front transients (in the order of hundreds of kilohertz) can be achieved by using one segment per coil. For very fast front transients (in the order of megahertz), one may require considering one segment per turn [12], [19].

The core inductance can be considered linear since high-frequency excitations yield reduced magnetic flux densities. Also, the flux penetration into the core can be neglected for very fast

Manuscript received November 23, 2009; revised April 10, 2010 and September 14, 2010; accepted December 20, 2010. Date of publication February 10, 2011; date of current version June 24, 2011. This work was supported in part by Secretaría de Investigación y Posgrado–Instituto Politécnico Nacional (SIP-IPN). Paper no. TPWRD-00865-2009.

P. Gómez is with the Electrical Engineering Department, SEPI-ESIME Zacatenco, Instituto Politécnico Nacional (IPN), Mexico City C. P. 07738, Mexico (e-mail: pgomez@ipn.mx).

F. de León is with the Department of Electrical and Computer Engineering, Polytechnic Institute, New York University, Brooklyn, NY 11201 USA (e-mail: fdeleon@poly.edu).

Color versions of one or more of the figures in this paper are available online at <http://ieeexplore.ieee.org>.

Digital Object Identifier 10.1109/TPWRD.2011.2104370

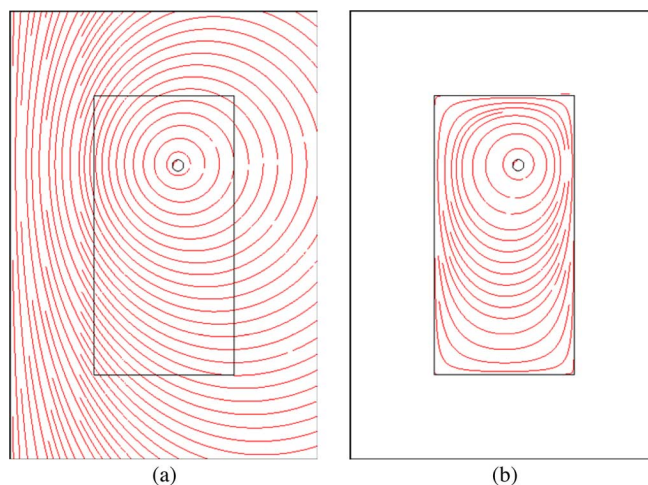


Fig. 1. Magnetic flux distribution at 10 MHz. (a) Air core. (b) Iron core.

front transients, such as those caused by switching operations in gas-insulated substations (GIS). At these high frequencies, the core acts as a flux barrier. The inductance matrix on a turn-to-turn basis is commonly computed by neglecting the existence of the core (i.e., by applying the formulae for air-core inductors) (see, for instance, [4], [7], and [15]–[17]). However, at very high frequencies (VHF), the core is closer to magnetic insulation (hollow material) than to an air-filled region. Therefore, the distribution of the magnetic field is quite different from that of an air-core inductor; this is more significant in the core window region as illustrated in Fig. 1 with finite-element (FEM) simulations. One can appreciate that the core window shapes the distribution of the magnetic flux, affecting the values of self and mutual inductances.

The most accurate way to take this into account when using computer methods is the application of electromagnetic-field simulations, which are able to consider the transformer geometry in great detail [9], [13]. Among the several numerical methods available for this purpose, the most commonly used approach is FEM analysis, which has proven to be very accurate. However, FEM analysis is, in general, computationally expensive and highly case dependent.

A technique to compute impedance values of winding coils at high frequencies without relying on FEM simulations is described in [14]. Since it is based on the rigorous solution of Maxwell's equations, it offers theoretically accurate results, but it also makes its implementation highly complicated.

The contribution of this paper is to present a technique, based on a multilayer method of images, to compute the inductance matrix of a transformer winding at very high frequencies without relying on FEM analysis. With a simple and straightforward algorithm, it is possible to obtain errors in the order of 1% (when compared with FEM) for all elements of the matrix. Moreover, self inductances and mutual inductances for neighboring turns, which define the most important values of the matrix, can be computed with high accuracy using a simple set of algebraic expressions instead of the more general algorithm.

Another important contribution of this paper is the uncovering of large errors incurred (around 40% for the self inductance and greater than 90% for the mutual inductances, for the test case analyzed) with the commonly used air-core formulae. Transient simulations demonstrate the accuracy of the proposed method and the incorrectness of the air-core approximation.

This paper is part of a work in progress aimed at obtaining high-frequency transformer models suitable for implementation in Electromagnetic Transients Program (EMTP)-type programs. For that reason, it is of paramount importance to compute the electrical parameters of the models with efficient, accurate, and easy-to-program expressions without relying on FEM simulations or complex algorithms.

II. METHOD OF IMAGES FOR INDUCTANCE CALCULATION

The method of images has been used for several decades in the computation of electromagnetic fields (emf) due to one or more sources under different boundary conditions [18]. The underlying idea is to replace a boundary by a fictitious source or set of sources with the correct magnitude, location, and form to obtain the emf solution accurately and efficiently.

As can be seen in Fig. 1, the behavior of the transformer core at very high frequencies approaches a magnetic insulating wall (the penetration of magnetic flux is minuscule). Two distinct regions can be identified for the inductance calculation: outside the core window and inside the core window. The total inductance is obtained by means of a weighted addition of the components from each region in direct proportion to the size. Therefore, the percentage of the winding in each region depends on the specific transformer geometry.

A. Outside the Core Window

Outside the window, the core leg can be represented by an infinite vertical line corresponding to a magnetic insulation boundary. This type of boundary can be replaced by conductor a carrying current I , corresponding to the winding turn, and an image b carrying current $-I$ used to replace the boundary; see Fig. 2. The image and actual conductors create the proper distribution of the magnetic flux density across the horizontal line joining the conductors and the core. To obtain the (self or mutual) inductance, one needs to compute the total flux linked by the turns from the integration of the flux density.

Considering a conductor with a circular cross-sectional area, the vertical component of the magnetic flux density from current I flowing through each element (per unit length) is given by

$$B_y = \frac{\mu_0 I}{2\pi x} \cos \theta \quad (1)$$

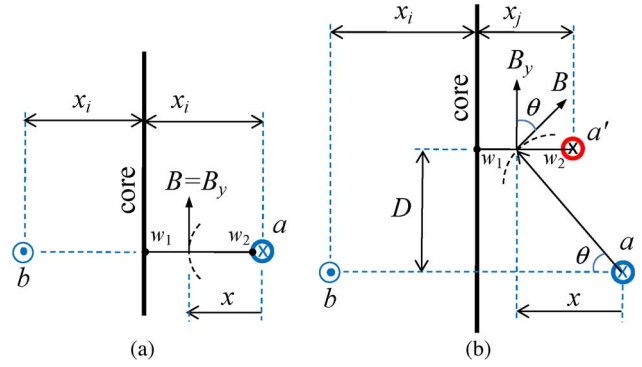


Fig. 2. Method of images to compute (a) the self inductance and (b) the mutual inductance outside the core window.

where μ_0 is the permeability of free space; angle θ is shown in Fig. 2(b) [$\theta = 0$ for Fig. 2(a)], and $2\pi x$ represents the variation of the magnetic flux perimeter along the integration contour delimited by w_1 and w_2 .

The self inductance of a turn outside the core window is obtained by taking into account the magnetic-field components from both carrying current conductors (a and b). Equation (1) is applied to compute the magnetic flux through the contour given by $w_1 \leq x \leq w_2$ due to each conductor

$$\psi = \frac{\mu_0 I}{2\pi} \int_{w_1}^{w_2} \frac{\cos \theta}{x} dx. \quad (2)$$

From (2), the total self flux of the i th turn, corresponding to the conductor a and its image b , is computed as

$$\psi_s = \frac{\mu_0 I}{2\pi} \ln \frac{2x_i - r}{r} \quad (3)$$

where r is the conductor radius. The self inductance per unit length is

$$L_s = \frac{\psi_s}{I} = \frac{\mu_0}{2\pi} \ln \frac{2x_i - r}{r}. \quad (4)$$

The mutual inductance between turns i and j outside the core window can be obtained by taking the flux components from conductor a into account and its image b crossing the contour corresponding to conductor a' , given again by $w_1 \leq x \leq w_2$. This is shown in Fig. 2(b). From (2) and (4), one obtains

$$L_m = \frac{\mu_0}{2\pi} \ln \frac{(x_j + x_i - r)^2 + D^2}{(x_j - x_i + r)^2 + D^2}. \quad (5)$$

B. Inside the Core Window

The four walls of a window can be replaced by the system of images shown in Fig. 3(a), considering the walls as reflective surfaces to locate the images. The conductor inside the core window, carrying current I , is denoted by a ; images b , c , d , and g , carrying current $-I$, are used to replace the four window walls; images e , g , h , and k , carrying current I , are included to reproduce the corners of the window.

The self inductance of the i th turn inside the core window is obtained by adding the magnetic-field components from each element of the system of images (including conductor a). From

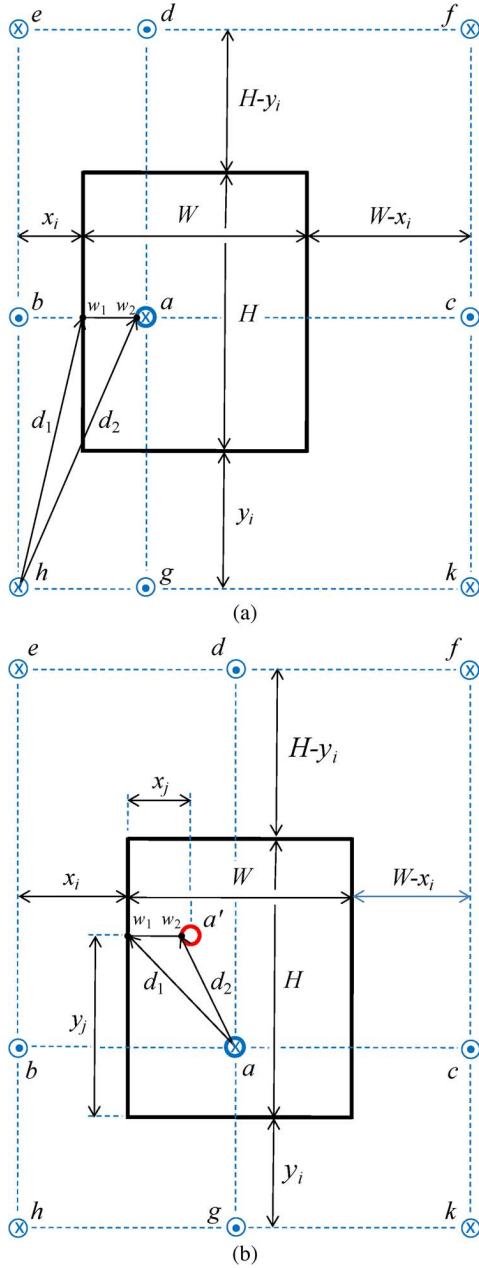


Fig. 3. Method of images to compute (a) the self inductance and (b) mutual inductance inside the core window.

(2), each magnetic flux component is computed in the general form

$$\psi = \frac{\mu_0 I}{2\pi} \ln \frac{d_1}{d_2} \quad (6)$$

where d_1 and d_2 are the distances between the center of the conductor and points w_1 and w_2 , respectively, as illustrated in Fig. 3(a) for image h . These distances are defined, in general, as follows:

$$d_1 = \sqrt{(x_i - x_{w_1})^2 + (y_i - y_{w_1})^2} \quad (7a)$$

$$d_2 = \sqrt{(x_i - x_{w_2})^2 + (y_i - y_{w_2})^2} \quad (7b)$$

where coordinates (x_{w_1}, y_{w_1}) and (x_{w_2}, y_{w_2}) define the location of points w_1 and w_2 , respectively. From (4), (6), and (7), a set of equations can be obtained for the inductive components of the whole system of images

$$L_a = \frac{\mu_0}{2\pi} \ln \frac{x_i}{r} \quad (8a)$$

$$L_b = \frac{\mu_0}{2\pi} \ln \frac{2x_i - r}{x_i} \quad (8b)$$

$$L_c = -\frac{\mu_0}{2\pi} \ln \frac{2W - x_i}{2W - 2x_i + r} \quad (8c)$$

$$L_d = -\frac{\mu_0}{4\pi} \ln \frac{x_i^2 + 4(H - y_i)^2}{r^2 + 4(H - y_i)^2} \quad (8d)$$

$$L_e = -\frac{\mu_0}{4\pi} \ln \frac{(2x_i - r)^2 + 4(H - y_i)^2}{x_i^2 + 4(H - y_i)^2} \quad (8e)$$

$$L_f = \frac{\mu_0}{4\pi} \ln \frac{(2W - x_i)^2 + 4(H - y_i)^2}{(2W - 2x_i + r)^2 + 4(H - y_i)^2} \quad (8f)$$

$$L_g = -\frac{\mu_0}{4\pi} \ln \frac{x_i^2 + 4y_i^2}{r^2 + 4y_i^2} \quad (8g)$$

$$L_h = -\frac{\mu_0}{4\pi} \ln \frac{(2x_i - r)^2 + 4y_i^2}{x_i^2 + 4y_i^2} \quad (8h)$$

$$L_k = \frac{\mu_0}{4\pi} \ln \frac{(2W - x_i)^2 + 4y_i^2}{(2W - 2x_i + r)^2 + 4y_i^2} \quad (8i)$$

The corresponding sign for each term depends on the direction of the current and the location of the image. The total self inductance L_s is computed as

$$L_s = L_a + L_b + L_c + L_d + L_e + L_f + L_g + L_h + L_k. \quad (9)$$

The mutual inductance between turns i and j inside the core window [Fig. 3(b)], is obtained by taking into account the flux components from conductor a and its images b to k , linking the contour corresponding to conductor a' . From (4), (6), and (7), these components are defined as

$$L_{a'a} = \frac{\mu_0}{4\pi} \ln \frac{x_j^2 + (y_j - y_i)^2}{(x_j - x_i + r)^2 + (y_j - y_i)^2} \quad (10a)$$

$$L_{a'b} = \frac{\mu_0}{4\pi} \ln \frac{(x_j + x_i - r)^2 + (y_j - y_i)^2}{x_j^2 + (y_j - y_i)^2} \quad (10b)$$

$$L_{a'c} = -\frac{\mu_0}{4\pi} \ln \frac{(2W - x_j)^2 + (y_j - y_i)^2}{(2W - x_j - x_i + r)^2 + (y_j - y_i)^2} \quad (10c)$$

$$L_{a'd} = -\frac{\mu_0}{4\pi} \ln \frac{x_j^2 + (2H - y_j - y_i)^2}{(x_j - x_i + r)^2 + (2H - y_j - y_i)^2} \quad (10d)$$

$$L_{a'e} = -\frac{\mu_0}{4\pi} \ln \frac{(x_j + x_i - r)^2 + (2H - y_j - y_i)^2}{x_j^2 + (2H - y_j - y_i)^2} \quad (10e)$$

$$L_{a'f} = \frac{\mu_0}{4\pi} \ln \frac{(2W - x_j)^2 + (2H - y_j - y_i)^2}{(2W - x_j - x_i + r)^2 + (2H - y_j - y_i)^2} \quad (10f)$$

$$L_{a'g} = -\frac{\mu_0}{4\pi} \ln \frac{x_j^2 + (y_j + y_i)^2}{(x_j - x_i + r)^2 + (y_j + y_i)^2} \quad (10g)$$

$$L_{a'h} = -\frac{\mu_0}{4\pi} \ln \frac{(x_j + x_i - r)^2 + (y_j + y_i)^2}{x_j^2 + (y_j + y_i)^2} \quad (10h)$$

$$L_{a'k} = \frac{\mu_0}{4\pi} \ln \frac{(2W - x_j)^2 + (y_j + y_i)^2}{(2W - x_j - x_i + r)^2 + (y_j + y_i)^2} \quad (10i)$$

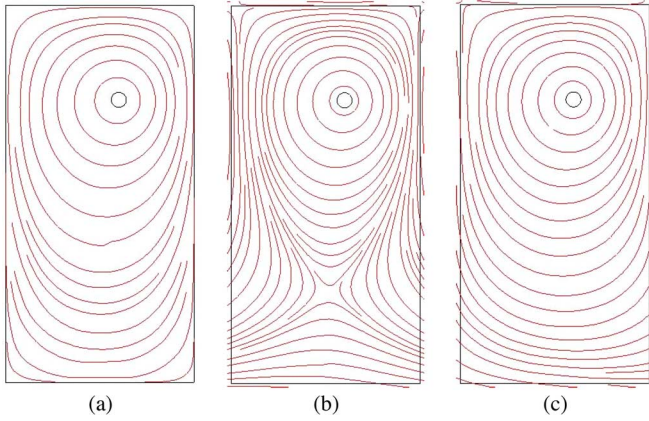


Fig. 4. Distribution of the magnetic flux inside the core window. (a) Real behavior at VHF. (b) Window replaced by one layer of images. (c) Window replaced by three layers of images.

The total mutual inductance L_m is computed from

$$L_m = L_{a'a} + L_{a'b} + L_{a'c} + L_{a'd} + L_{a'e} + L_{a'f} + L_{a'g} + L_{a'h} + L_{a'k} \quad (11)$$

III. GENERALIZED METHOD OF IMAGES FOR THE MUTUAL INDUCTANCE INSIDE THE CORE WINDOW

In the strict sense, images created by the conductor inside the core window give rise to images on the other side of the geometry (images of images) and so forth. The number of layers of images required to accurately reproduce the magnetic flux inside the core window depends on the effect that these images have on the correct reproduction of the boundaries they replace. In general, computation of the self inductance requires only first-order images, as described in Section II-B. However, it was found that for mutual inductances, the number of layers of images required to reproduce the magnetic-field distribution with fidelity, depends on the separation between conductors. This can be explained with the help of Fig. 4, which shows the magnetic flux distribution from one circular conductor under three different conditions. Fig. 4(a) shows the actual behavior of the flux at very high frequencies (obtained with FEM). After replacing the core window by one layer of images, the flux distribution is illustrated in Fig. 4(b). The flux distribution is reproduced correctly for the region closer to the conductor, but it deviates from the actual flux as the distance increases. As seen in Fig. 4(c), a better approximation to the actual behavior at VHF is obtained after including two more layers of images. Nevertheless, it is observed that the field far from the source flux is not perfectly reproduced with three layers of images.

A general algorithm to compute the mutual flux in a more accurate manner is obtained by successively applying (6) and (7), adding layers of images one at a time and computing the relative difference between consecutive values. The algorithm stops when the difference is lower than a fixed quantity ε . A detailed description of the process is depicted in Fig. 5. This

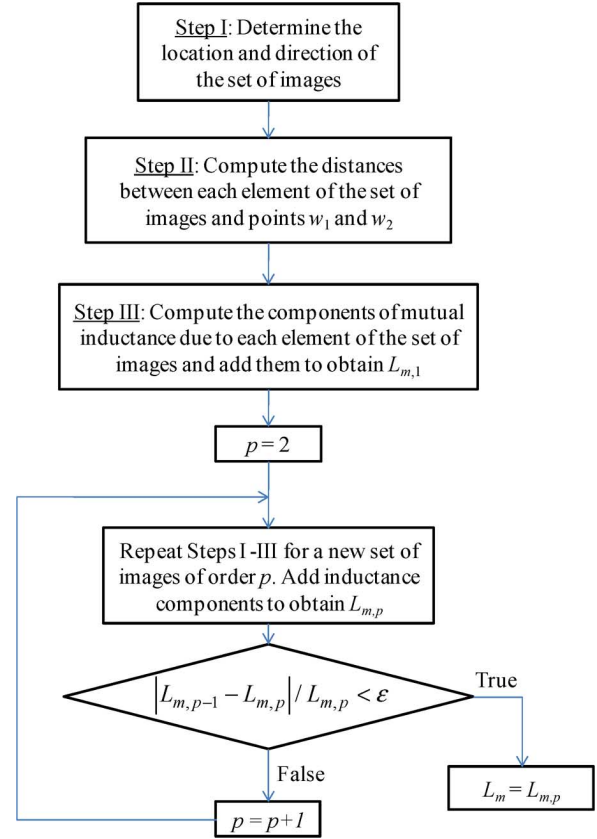


Fig. 5. Flowchart of the process to obtain the mutual inductance using multiple layers of images for each turn.

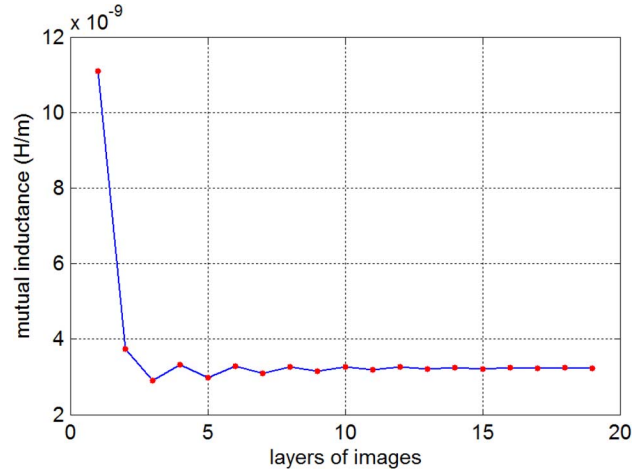


Fig. 6. Mutual inductance as the number of layers of images is increased.

method can be further improved by computing the average of consecutive values prior to computing the relative difference.

The convergence properties of the mutual inductance calculation are shown in Fig. 6 for a simple arrangement consisting of 2 conductors with coordinates (0.1,0.025), (0.2,0.275) from the low left corner of a core window of dimensions 0.3×0.3 , all in meters. Fig. 7 shows the relative error. For this case, 19 layers of images were required to obtain a relative difference lower than 1%.

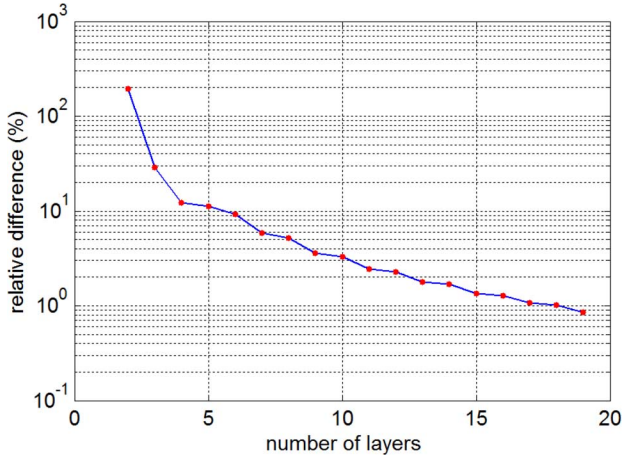


Fig. 7. Relative difference between consecutive values of mutual inductance.

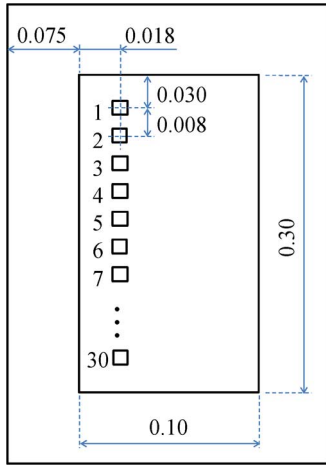


Fig. 8. Geometrical configuration of the transformer.

IV. TEST CASE

The transformer winding shown in Fig. 8 is applied to test the method described in this paper. It consists of 30 turns with a square cross-sectional area of $4 \text{ mm} \times 4 \text{ mm}$. The distance between centers of contiguous turns is 8 mm. The core material is silicon steel with a conductivity of $2.08 \times 10^6 \text{ S/m}$ and a relative permeability of 50 000. The core window dimensions are $W = 0.1 \text{ m}$, $H = 0.3 \text{ m}$.

FEM simulations were performed using the commercially available software COMSOL Multiphysics [21]. A script was developed to obtain the entire set of self and mutual inductances by applying the magnetic energy method [19].

A. Single Layer of Images

Tables I and II show representative values for the self and mutual inductance outside the core window, respectively. They have been computed with the analytical formulae given in Section II-A and compared with FEM simulations at frequencies of 10, 1, and 0.1 MHz. Included in both tables is the case when the core wall is replaced by a magnetic insulation boundary using FEM. Relative differences between results are given (relative to the FEM results in all cases). Although only a few digits are

TABLE I
PERCENT DIFFERENCE IN THE SELF INDUCTANCE OUTSIDE THE CORE WINDOW

Self L	Method of Images	FEM Magnetic Insulation	FEM 10 MHz	FEM 1 MHz	FEM 0.1 MHz
		[μH]	[%]		
$L_{1,1}$	0.5410	0.24	0.14	1.19	24.50
$L_{2,2}$		0.23	0.13	1.17	24.98
$L_{3,3}$		0.25	0.13	1.16	25.24
$L_{4,4}$		0.24	0.13	1.15	25.27
$L_{5,5}$		0.23	0.13	1.14	25.16
$L_{6,6}$		0.22	0.13	1.15	25.16
$L_{7,7}$		0.23	0.12	1.13	24.91
$L_{9,9}$		0.22	0.12	1.13	24.74
$L_{12,12}$		0.25	0.12	1.14	24.72
$L_{15,15}$		0.19	0.12	1.14	24.61
$L_{17,17}$		0.22	0.12	1.12	24.47
$L_{21,21}$		0.18	0.12	1.12	24.31
$L_{30,30}$		0.20	0.13	1.11	24.33

TABLE II
PERCENT DIFFERENCE IN THE MUTUAL INDUCTANCE OUTSIDE THE CORE WINDOW

Mutual L	Method of Images	FEM Magnetic Insulation	FEM 10 MHz	FEM 1 MHz	FEM 0.1 MHz
		[μH]	[%]		
$L_{1,2}$	0.2857	1.12	1.11	2.97	40.61
$L_{1,3}$	0.1676	0.83	0.81	3.68	53.37
$L_{1,4}$	0.1082	0.86	0.83	4.37	62.21
$L_{1,5}$	0.0743	0.95	0.90	4.80	68.29
$L_{1,6}$	0.0534	1.05	0.98	5.03	72.51
$L_{1,7}$	0.0399	1.17	1.07	5.16	75.49
$L_{1,9}$	0.0244	1.40	1.26	5.32	79.18
$L_{1,12}$	0.0137	1.78	1.58	5.48	81.74
$L_{1,15}$	0.0087	2.21	1.94	5.75	82.66
$L_{1,17}$	0.0067	2.52	2.21	5.94	82.79
$L_{1,21}$	0.0043	3.23	2.81	6.37	82.41
$L_{1,30}$	0.0021	5.67	4.85	8.13	79.66

shown in the results, the relative differences are computed using full precision.

Tables III and IV show selected values for the self and mutual inductances inside the core window, respectively. These have been computed with the method of images (considering only one layer of images) and compared with FEM simulations. Relative differences between the results are included.

It can be noticed from Tables I–IV that the results are virtually equal considering a very high frequency (10 MHz) or imposing magnetic insulation boundaries to the core internal walls. One can also observe that the results for the self inductance are in very close agreement to FEM simulations at 1 and 10 MHz, with differences always smaller than 1.8%. However, this is not the case for the mutual inductances (particularly inside the core window). It can be seen from Table IV that the relative difference increases with the separation distance.

TABLE III
PERCENT DIFFERENCE IN THE SELF INDUCTANCE
INSIDE THE CORE WINDOW

Self L	Method of Images	FEM Magnetic Insulation	FEM 10 MHz	FEM 1 MHz	FEM 0.1 MHz
	[μH]	[%]			
L _{1,1}	0.5130	0.37	0.17	0.77	19.60
L _{2,2}	0.5216	0.13	0.04	1.02	20.05
L _{3,3}	0.5259	0.00	0.18	1.16	20.86
L _{4,4}	0.5282	0.13	0.27	1.27	21.62
L _{5,5}	0.5294	0.17	0.35	1.36	22.21
L _{6,6}	0.5300	0.26	0.43	1.43	22.65
L _{7,7}	0.5302	0.34	0.49	1.49	22.95
L _{9,9}	0.5301	0.39	0.60	1.59	23.29
L _{12,12}	0.5298	0.54	0.72	1.72	23.55
L _{15,15}	0.5295	0.60	0.77	1.78	23.63
L _{17,17}	0.5295	0.61	0.78	1.77	23.59
L _{21,21}	0.5299	0.52	0.69	1.65	23.17
L _{30,30}	0.5216	0.18	0.04	0.95	19.50

TABLE IV
PERCENT DIFFERENCE IN THE MUTUAL INDUCTANCE INSIDE THE CORE
WINDOW (SINGLE LAYER OF IMAGES)

Mutual L	Method of Images	FEM Magnetic Insulation	FEM 10 MHz	FEM 1 MHz	FEM 0.1 MHz
	[μH]	[%]			
L _{1,2}	0.2628	0.52	0.55	2.28	35.71
L _{1,3}	0.1483	0.07	0.10	2.90	49.63
L _{1,4}	0.0917	0.15	0.12	3.44	59.67
L _{1,5}	0.0598	0.40	0.36	3.66	66.80
L _{1,6}	0.0406	0.70	0.67	3.63	71.92
L _{1,7}	0.0285	1.10	1.06	3.39	75.70
L _{1,9}	0.0150	2.27	2.23	2.39	80.80
L _{1,12}	0.0065	6.13	6.09	1.09	85.23
L _{1,15}	0.0032	17.87	17.82	12.02	87.36
L _{1,17}	0.0022	37.68	37.62	30.63	87.49
L _{1,21}	0.0015	165.69	165.57	150.94	82.62
L _{1,30}	0.0022	3935.2	3932.70	3679.00	29.13

The last two columns of Tables I–IV show that at 0.1 MHz, the influence of the core produces an important increase in the inductance values. This effect is not considered by the analytical method proposed in this paper and, therefore, its application should remain in the megahertz frequency range.

B. Multiple Layer of Images

As shown before, the mutual inductance calculation can be enhanced by applying the method described in Section III. The number of layers of images is increased until the relative difference between consecutive values is lower than 0.1%. The results are shown in Table V. One can see that the computation accuracy is greatly enhanced by the use of multiple layers of images.

TABLE V
MUTUAL INDUCTANCE INSIDE THE CORE WINDOW
(MULTIPLE LAYERS OF IMAGES)

Mutual L	Method of Images [μH]	FEM 10 MHz [μH]	Diff (%)	Images (layers)
L _{1,2}	0.26196	0.26421	0.85	6
L _{1,3}	0.14755	0.14843	0.59	6
L _{1,4}	0.09099	0.09155	0.61	8
L _{1,5}	0.05920	0.05959	0.65	8
L _{1,6}	0.04006	0.04034	0.70	10
L _{1,7}	0.02796	0.02816	0.72	10
L _{1,9}	0.01455	0.01466	0.76	14
L _{1,12}	0.00606	0.00611	0.79	20
L _{1,15}	0.00269	0.00271	0.79	28
L _{1,17}	0.00160	0.00161	0.79	36
L _{1,21}	0.00057	0.00058	0.79	60
L _{1,30}	0.00005	0.00005	0.76	194

TABLE VI
FEM SELF INDUCTANCE VERSUS AIR-CORE INDUCTANCE

Self L	FEM 10 MHz [μH]	Air-core [μH]	Error (%)
L _{1,1}	0.5122	0.7298	42.49
L _{2,2}	0.5218		39.87
L _{3,3}	0.5268		38.53
L _{4,4}	0.5297		37.79
L _{5,5}	0.5313		37.37
L _{6,6}	0.5322		37.12
L _{7,7}	0.5328		36.97
L _{9,9}	0.5333		36.83
L _{12,12}	0.5336		36.77
L _{15,15}	0.5336		36.76
L _{17,17}	0.5336		36.76
L _{21,21}	0.5335		36.79
L _{30,30}	0.5217		39.88

C. Air-Core Inductances

The comparison between the inductance values (self and mutual) inside the core window (computed using FEM) and the traditional air-core approximation is shown in Tables VI and VII. Note that the air-core assumption overestimates the self inductance by around 40%, while the mutual inductance is overestimated by more than 90% with much larger errors as the distance between turns increases.

V. DISCUSSION

Table IV shows that when using only one layer of images, the mutual inductances for turns that are fairly separated are computed with large errors. Nonetheless, these values are several orders of magnitude smaller than the values obtained between contiguous turns. Since the largest inductances dominate the transient response of the winding, the influence of the much smaller mutual inductances becomes negligible.

TABLE VII
FEM MUTUAL INDUCTANCE VERSUS AIR-CORE INDUCTANCE

Mutual L	FEM 10 MHz [μH]	Air-core [μH]	Error (%)
$L_{1,2}$	0.26421	0.51479	94.84
$L_{1,3}$	0.14843	0.38345	158.33
$L_{1,4}$	0.09155	0.30606	234.32
$L_{1,5}$	0.05959	0.25246	323.68
$L_{1,6}$	0.04034	0.21239	426.49
$L_{1,7}$	0.02816	0.18114	543.30
$L_{1,9}$	0.01466	0.13564	825.11
$L_{1,12}$	0.00611	0.09264	1416.39
$L_{1,15}$	0.00271	0.06637	2344.65
$L_{1,17}$	0.00161	0.05430	3273.69
$L_{1,21}$	0.00058	0.03796	6475.46
$L_{1,30}$	0.00005	0.01985	36582.72

Consider the same geometrical arrangement of Section IV (Fig. 8). The complete inductance matrix \mathbf{L} is computed in two ways: 1) using only one layer of images, as described in Section II-B and 2) with multiple layers of images, as explained in Section III. Then, the capacitance matrix \mathbf{C} is computed from the inverse of the inductance matrix and the constitutive parameters. From these two matrices, a nodal system of equations describing the winding can be obtained, as detailed in the Appendix.

The response of the winding to a fast front transient is obtained by injecting a unit-square pulse (width: 32.2 ns) at the beginning of the winding, with the far end grounded. A lossless case is assumed, and only the region inside the core window is considered. This makes the simulation case merely theoretical, but it allows properly gauging the differences between the two techniques used to compute the inductance matrix inside the core window. In a practical case, the appropriate estimation of losses would be required. The method can be used in conjunction with the dc inductance to compute the losses and inductance at any frequency as is commonly done with transmission-line modeling [22]. This is possible since the variation with the frequency of core and winding impedances follows regular (known) patterns [23], [24]. The issue will be tackled in a forthcoming paper.

Fig. 9(a) shows the transient voltage response of the winding at turn 7, where the maximum overvoltage occurs. Fig. 9(b) and (c) shows the transient response at turns 12 and 25. It can be seen from all figures that the results with one layer and with multiple layers of images are almost identical. Fig. 9 also includes comparisons with the waveforms obtained when computing the inductances with the air-core approximation. The large errors introduced in the computation of transients when neglecting the core effects are evident. Similar results are obtained for the remaining turns (not shown).

It can be concluded from the test that only one layer of images is required to compute the transient response of the winding with enough accuracy for most cases. This is so because the inductance elements of neighboring turns are adequately obtained. Equations (8) and (10) are very simple expressions that can be

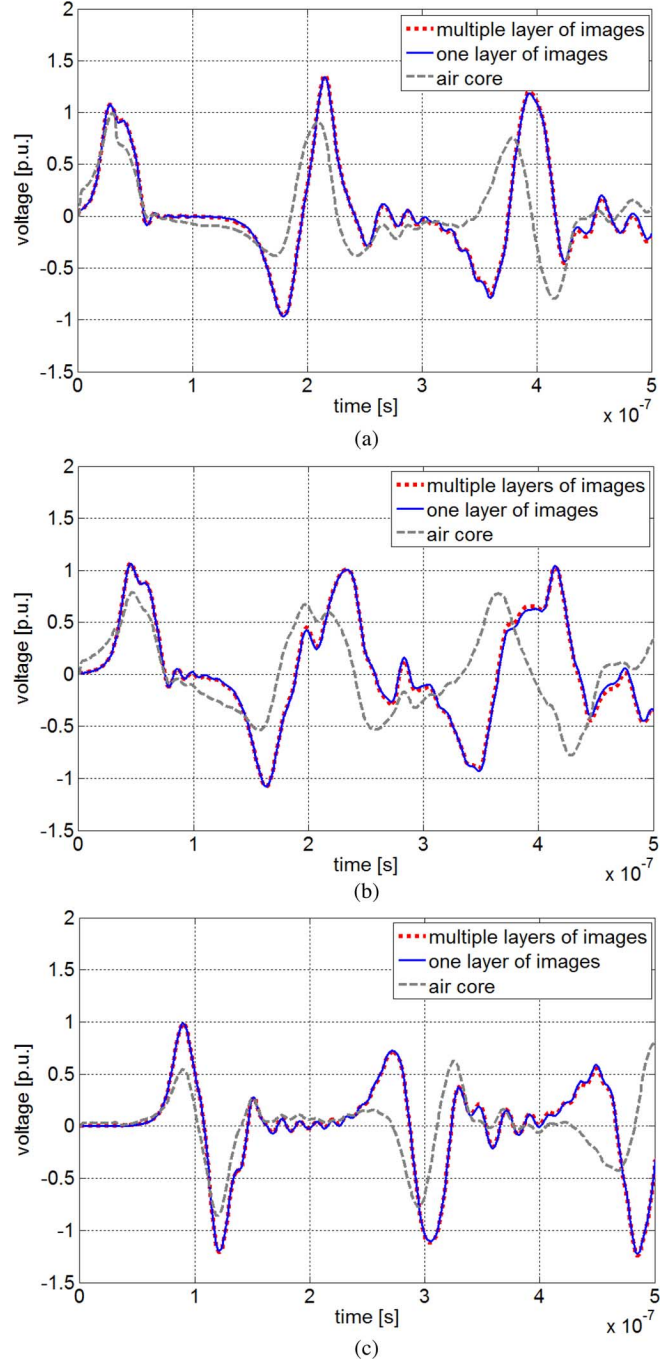


Fig. 9. Transient response of the winding to a unit-square pulse. (a) At turn 7. (b) At turn 12. (c) At turn 25.

easily implemented in EMTP-type programs as part of the parameter computation for very fast transients in transformers.

VI. CONCLUSION

This paper has presented a simple and efficient procedure to compute the inductance matrix of a transformer winding for the simulation of very fast transients. The procedure is based on the application of the method of images considering that the transformer core behaves like a magnetic insulation boundary at very high frequencies (megahertz). Expressions for the self and mutual inductances in the regions inside and outside the core

window have been given. An algorithm has been developed to consider more than one layer of images for the calculation of mutual inductances inside the core window.

The following conclusions are obtained from the implementation and application of the procedure:

- 1) Self and mutual inductances outside the core window are computed with high accuracy (using one image) with the straightforward (4) and (5).
- 2) For the self inductances inside the core window, applying the set of equations (8), corresponding to a single layer of images, results in very accurate values. Therefore, further layers of images are not required. This is because the self inductance is computed from the magnetic flux between the turn and the core, and this is properly reproduced with a single layer of images.
- 3) The calculation error of mutual inductances inside the core window with a single layer of images increases as the distance between turns increases. By adding more layers of images, it is possible to compute mutual inductances with high accuracy regardless of their positions inside the core window.
- 4) By means of a simulation example, it was shown that the errors in the computation of mutual inductance values with one layer of images have almost no effect in the transient response of the winding at very high frequencies. Therefore, the inclusion of more layers of images is, in general, not required, although this depends on the aspect ratio of the transformer window and the conductors' position inside the window.
- 5) Very large errors have been revealed when computing the self and mutual inductances with the commonly used air-core approximations. The consequence of this is that the transient response of a winding is not properly computed when the core is represented as air.

APPENDIX

After computing the winding inductance matrix \mathbf{L} , the capacitance matrix is obtained as

$$\mathbf{C} = \mu_0 \varepsilon \mathbf{L}^{-1} \quad (12)$$

where ε is the permittivity of the surrounding medium. From \mathbf{L} and \mathbf{C} , a nodal system can be defined to describe the winding (Fig. 10)

$$\mathbf{I}(s) = \mathbf{Y}(s)\mathbf{V}(s) \quad (13)$$

where $\mathbf{V}(s)$ and $\mathbf{I}(s)$ correspond to the vectors of nodal voltages and currents; and $\mathbf{Y}(s)$ is the nodal admittance matrix which, for a lossless system, is defined as follows [2]:

$$\mathbf{Y}(s) = \mathbf{C}s + \frac{\mathbf{\Gamma}}{s} \quad (14)$$

where $\mathbf{\Gamma}$ is the nodal matrix of inverse inductances, computed from \mathbf{L} and the incidence matrix \mathbf{K} (since \mathbf{L} is a branch matrix)

$$\mathbf{\Gamma} = \mathbf{K}\mathbf{L}^{-1}\mathbf{K}^t \quad (15)$$

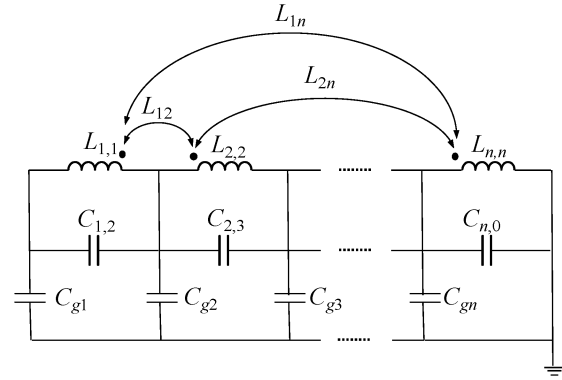


Fig. 10. Circuitual representation of a lossless transformer winding. Mutual capacitances between noncontiguous segments are omitted for the sake of simplicity.

where

$$\mathbf{K} = \begin{bmatrix} 1 & 0 & 0 & \cdots & 0 & 0 \\ -1 & 1 & 0 & \cdots & 0 & 0 \\ 0 & -1 & 1 & \cdots & 0 & 0 \\ \vdots & \vdots & \vdots & \ddots & \vdots & \vdots \\ 0 & 0 & 0 & \cdots & 1 & 0 \\ 0 & 0 & 0 & \cdots & -1 & 1 \end{bmatrix}. \quad (16)$$

Finally, the time-domain response is obtained by applying the inverse numerical Laplace transform [20].

REFERENCES

- [1] L. Rabins, "A new approach to the analysis of impulse voltages and gradients in transformer windings," *AIEE Trans.*, vol. 78, no. 4, pp. 1784–1791, Feb. 1960.
- [2] P. I. Fergestad and T. Henriksen, "Transient oscillations in multi-winding transformers," *IEEE Trans. Power App. Syst.*, vol. PAS-93, no. 2, pp. 500–509, Mar./Apr. 1974.
- [3] W. J. Mc Nutt, T. J. Blalock, and R. A. Hinton, "Response of transformer windings to system transient voltages," *IEEE Trans. Power App. Syst.*, vol. PAS-93, no. 2, pp. 457–466, Mar./Apr. 1974.
- [4] A. Miki, T. Hosoya, and K. Okuyama, "A calculation method for impulse voltage distribution and transferred voltage in transformer windings," *IEEE Trans. Power App. Syst.*, vol. PAS-97, no. 3, pp. 930–939, May/Jun. 1978.
- [5] K. J. Cornick, B. Filliat, C. Kieny, and W. Muller, "Distribution of very fast transient overvoltages in transformer windings," *CIGRE Rep. 1992*, pp. 12–204.
- [6] Y. Shibuya, S. Fujita, and N. Hosokawa, "Analysis of very fast transient overvoltage in transformer winding," *Proc. Inst. Elect. Eng., Gen. Transm. Distrib.*, vol. 144, no. 5, Sep. 1997.
- [7] Y. Shibuya, S. Fujita, and E. Tamaki, "Analysis of very fast transients in transformer," *Proc. Inst. Elect. Eng., Gen. Transm. Distrib.*, vol. 148, no. 5, pp. 377–383, 2001.
- [8] M. Popov, L. V. Sluis, G. C. Paap, and H. de Herdt, "Computation of very fast transient overvoltages in transformer windings," *IEEE Trans. Power Del.*, vol. 18, no. 4, pp. 1268–1274, Oct. 2003.
- [9] E. Bjerkan and H. K. Høidalen, "High frequency fem-based power transformer modeling: Investigation of internal computation of very fast transient overvoltages in transformer windings due to network-initiated overvoltages," presented at the Int. Conf. Power Syst. Transients, Montreal, QC, Canada, Jun. 19–23, 2005.
- [10] G. Liang, H. Sun, X. Zhang, and X. Cui, "Modeling of transformer windings under very fast transient overvoltages," *IEEE Trans. Electro-magn. Compat.*, vol. 48, no. 4, pp. 621–627, Nov. 2006.
- [11] M. Popov, L. van der Sluis, R. P. P. Smeets, and J. Lopez Roldan, "Analysis of very fast transients in layer-type transformer windings," *IEEE Trans. Power Del.*, vol. 22, no. 1, pp. 238–247, Jan. 2007.

- [12] S. M. H. Hosseini, M. Vakilian, and G. B. Gharehpetian, "Comparison of transformer detailed models for fast and very fast transient studies," *IEEE Trans. Power Del.*, vol. 23, no. 2, pp. 733–741, Apr. 2008.
- [13] Z. Azzouz, A. Foggia, L. Pierrat, and G. Meunier, "3D finite element computation of the high frequency parameters of power transformer windings," *IEEE Trans. Magn.*, vol. 29, no. 2, pp. 1407–1410, Mar. 1993.
- [14] D. J. Wilcox, M. Conlon, and W. G. Hurley, "Calculation of self and mutual impedances for coils on ferromagnetic cores," *Proc. Inst. Elect. Eng.*, vol. 135, no. 7, pp. 470–476, Sep. 1988, h A.
- [15] R. M. Del Vecchio, B. Poulin, and R. Ahuja, "Calculation and measurement of winding disk capacitances with wound-in-shields," *IEEE Trans. Power Del.*, vol. 13, no. 2, pp. 503–509, Apr. 1998.
- [16] A. Greenwood, *Electrical Transients in Power Systems*. New York: Wiley, 1991, pp. 424–431.
- [17] S. V. Kulkarni and S. A. Khaparde, *Transformer Engineering: Design and Practice*. Boca Raton, FL: CRC, 2004, pp. 298–299.
- [18] L. V. Bewley, *Two-Dimensional Fields in Electrical Engineering*. New York: Dover, 1963, pp. 151–166.
- [19] F. de León, P. Gómez, J. A. Martínez-Velasco, and M. Rioual, J. A. Martínez-Velasco, Ed., "Transformers," in *Power System Transients: Parameter Determination*. Boca Raton, FL: CRC, 2009, ch. 4, pp. 177–250.
- [20] P. Gómez and F. A. Uribe, "The numerical laplace transform: An accurate tool for analyzing electromagnetic transients on power system devices," *Int. J. Elect. Power Energy Syst.*, vol. 31, no. 2, pp. 116–123, Feb./Mar. 2009.
- [21] COMSOL AB, COMSOL Multiphysics User's Guide. Nov. 2008. [Online]. Available: <http://www.comsol.com/>
- [22] A. Semlyen and A. Deri, "Time domain modelling of frequency dependent three-phase transmission line impedance," *IEEE Trans. Power App. Syst.*, vol. PAS-104, no. 6, pp. 1549–1555, Jun. 1985.
- [23] R. L. Stoll, *The Analysis of Eddy Currents*. London, U.K.: Oxford Univ. Press, 1974.
- [24] F. de León and A. Semlyen, "Time domain modeling of eddy current effects for transformer transients," *IEEE Trans. Power Del.*, vol. 8, no. 1, pp. 271–280, Jan. 1993.

Pablo Gómez (M'10) was born in Zapopan, México, in 1978. He received the B.Sc. degree in mechanical and electrical engineering from Universidad Autónoma de Coahuila, Mexico, in 1999, and the M.Sc. and Ph.D. degrees in electrical engineering from CINVESTAV, Guadalajara, Mexico, in 2002 and 2005, respectively.

Since 2005, he has been a Full-Time Professor with the Electrical Engineering Department, SEPI-ESIME Zacatenco, National Polytechnic Institute, Mexico City. From 2008 to 2010, he was on postdoctoral leave at the Polytechnic Institute, New York University, Brooklyn, NY. His research interests are modeling and simulation for electromagnetic transient analysis and electromagnetic compatibility.

Francisco de León (S'86-M'92-SM'02) received the B.Sc. and M.Sc. degrees in electrical engineering from the National Polytechnic Institute, Mexico, in 1983 and 1986, respectively, and the Ph.D. degree from the University of Toronto, Toronto, ON, Canada, in 1992.

He has held several academic positions in Mexico and has worked for the Canadian electric industry. Currently, he is an Associate Professor at the Polytechnic Institute of New York University, Brooklyn, NY. His research interests include the analysis of power phenomena under nonsinusoidal conditions, the transient and steady-state analyses of power systems, the thermal rating of cables, and the calculation of electromagnetic fields applied to machine design and modeling.